CrystEngComm

ROYAL SOCIETY OF CHEMISTRY

PAPER

View Article Online
View Journal | View Issue

Cite this: *CrystEngComm*, 2022, **24**, 5757

Bonding and uneven charge distribution in infinite pyrene π-stacks†

Chase Flynn,[a] Zheng Zhou,[bc] Megan E. McCormack,[b] Zheng Wei,[b] Marina A. Petrukhina *[b] and Miklos Kertesz *[a]

Unusual intermolecular π-stacking in a new charge transfer salt of pyrene (Py), $(Py)_2^+(Ga_2Cl_7)^-$, has been observed. The structure obtained by single crystal X-ray crystallography indicates π-stacks of pyrene which were analyzed using a combination of density functional theory and the analysis of the bond length alternation patterns in the pyrene molecules in different charge states. There are relatively few crystal structures of charge transfer salts of pyrene in the literature, and this structure shows a unique charge separation in which half of the pyrenes are nearly neutral while the other half carry approximately +1 charge in an alternating fashion along the 1D stacks balancing one electron charge transfer to each $(Ga_2Cl_7)^-$ anion. The charge localization is attributed to the incomplete inter-pyrene overlap of the singly occupied molecular orbitals.

Received 6th July 2022,
Accepted 8th July 2022

DOI: 10.1039/d2ce00933a

rsc.li/crystengcomm

Introduction

Charge transfer salts of organic conjugated molecules display richness of intermolecular interactions identified by X-ray diffraction (XRD). The degree of charge transfer (CT) depends on a number of circumstances, which were discussed in detail in connection with highly conducting CT salts,[1] *e.g.* TTF–TCNQ (TTF is tetrathiafulvalene, and TCNQ is tetracyanoquinodimethane). The main driving force is the energy gain obtained from the difference of the ionization potential of the donor and the electron affinity of the acceptor, the resulting Coulomb interactions as represented by the Madelung energy[2] of the crystal, and the delocalization energy (if present) along the intermolecular π–π overlap that can create metallic-like energy bands, dispersion interactions, and crystal packing.[3,4] The resulting singly occupied molecular orbitals (SOMOs) play a central role in two ways: through intermolecular overlap they can provide both stabilization *via* multiple centre covalent bonding between open-shell extended π-electron species called for short "pancake bonding"[5,6] and pathways for extended electron delocalization.[7] A few examples are shown in Scheme 1, some neutral and some charged monomers that form these shorter than van der Waals contacts that also go hand in hand with atom-over-atom configurations. This critical orbital is the highest occupied molecular orbital (HOMO) that becomes the SOMO in the cation radical. There are six regions in the SOMO of the pyrene molecule with the characteristics of a bonding combination, localized around bonds r_2 and r_5, providing six regions in pyrene for intermolecular in-phase pancake bonding. The atomic numbering and the relevant orbital for pyrene are shown in Scheme 2. Various well-

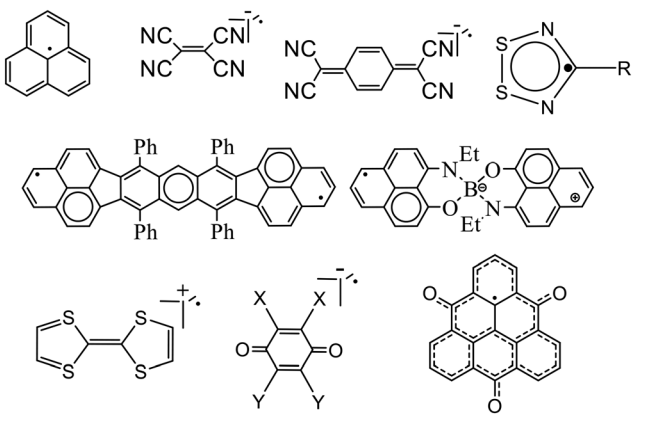

Scheme 1 Select examples of molecules that form pancake bonds, multiple centre covalent bonding between open-shell extended π-electron species. For clarity side groups are omitted. Charges are indicated on a per monomer basis. Examples of partial charges on average are common.

[a] *Chemistry Department and Institute of Soft Matter, Georgetown University, 37th and O Streets, NW, Washington DC 20057-1227, USA.*
E-mail: kertesz@georgetown.edu
[b] *Department of Chemistry, University at Albany, State University of New York, 1400 Washington Avenue, Albany, NY 12222, USA.*
E-mail: mpetrukhina@albany.edu
[c] *School of Materials Science and Engineering, Tongji University, 4800 Cao'an Road, Shanghai 201804, China*

† Electronic supplementary information (ESI) available. CCDC 2169170. For ESI and crystallographic data in CIF or other electronic format see DOI: https://doi.org/10.1039/d2ce00933a

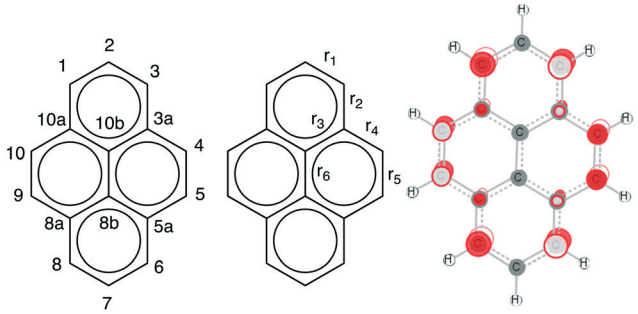

Scheme 2 Pyrene molecules with carbon atoms numbered, unique bonds labelled r_1 through r_6, and the HOMO of pyrene, which is the SOMO of the $(Py)^+$ cation.

overlapping combinations with a relative slip and/or rotation can occur in addition to the fully overlapping stable minimum discussed by Devic *et al.*[8]

The number of electron pairs available for the SOMO–SOMO bonding interaction defines the formal intermolecular pancake bond order, PBO:

$$\mathrm{PBO} = 1/2(N_{\mathrm{bind}} - N_{\mathrm{anti}}), \quad (1)$$

where N_{bind} and N_{anti} are the number of bonding and antibonding electrons in the SOMO based orbital manifold, respectively.[6]

Fig. 1 illustrates a case of PBO = 1/2; cases of pancake bonding with both PBO ≥ 1 (ref. 9) and PBO < 1 (ref. 10 and 11) are known. It is an interesting characteristic of pancake bonding, that under the right circumstances, its strength may be larger for dimers with a smaller PBO, due to the interplay of the components of the intermolecular interaction: SOMO–SOMO interaction, dispersion, electrostatic interaction, and hydrogen bonding if present.[11,12] One of the goals of the present work is to reveal the factors affecting the nature of pancake bonding in polycyclic aromatic hydrocarbons (PAHs).

The delocalization energy between two π-stacking organic conjugated molecules can arise in several ways. The simplest

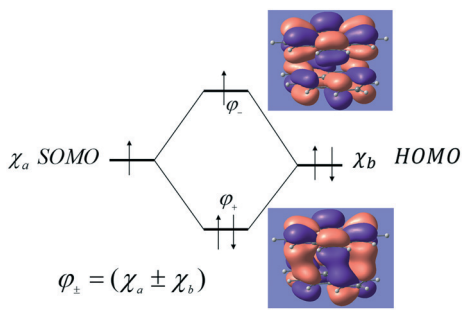

Fig. 1 SOMO–HOMO interaction diagram of $(Py)_2^+$, a radical cation dimer. The bonding combination of these two orbitals yields the HOMO (φ_+) of the dimer, and the antibonding interaction yields the SOMO of the dimer. The net formal pancake bond order for the dimer is 1/2. Orbitals for the most stable 60° rotated configuration are shown, see Table 1.

occurs in the case of one unpaired electron per molecule where the resulting "pancake" interaction can create a relatively stable closed shell dimer. The prototypical pancake bond for the neutral phenalenyl radical dimer[13] has one electron on each SOMO yielding PBO = 1. In the case of the title system, there are two donors per one acceptor, there are three electrons in the SOMO orbital space and effectively only one electron contributing to the stabilization of a dimer in the crystal, as illustrated in Fig. 1.

Pancake bonding arises from the sharing of electrons in an intermolecular multicenter bond with π-stacking geometry where the atoms contributing π-electrons are in perfect or nearly perfect atom-over-atom coordination.[6,13] This stabilizing interaction is to be contrasted with van der Waals interaction where the typical π-stacking geometry is characterized by the avoidance of atom-over-atom coordination in order to reduce steric repulsions. As a general trend, Devic *et al.* obtained the "Maximin Principle" based on the preference of maximum overlap for one or two electrons sharing the delocalized intermolecular orbital originating in the SOMOs of the molecules and at the same time a minimum contact of carbon atoms not participating in the SOMO.[8] Further characteristics of pancake bonding include low singlet–triplet and singlet–singlet excitation energies and interaction energies that significantly exceed that of vdW interaction for comparable size systems.[12]

In this work, unusual intermolecular π-stacking of pyrene has been crystallographically revealed in the new product, $(Py)_2^+(Ga_2Cl_7)^-$. This has prompted us to carry out comprehensive theoretical investigations of bonding and charge distribution patterns using a diverse set of computational tools. Our main objective is to evaluate if the observed packing represents a case of ideal or near ideal π-stacking overlap for pancake bonding.

Results and discussion

Preparation and crystallographic study of $(Py)_2^+(Ga_2Cl_7)^-$

In this work, mixing pyrene and $GaCl_3$ in a 1:2 ratio in anhydrous fluorobenzene at room temperature under an inert atmosphere afforded a golden-brown solution. Crystals suitable for X-ray diffraction were grown through cooling of the solution to −5 °C to produce large brown needles in 70% yield after two weeks. The X-ray diffraction experiment confirmed the formation of a new product with the composition of $(Py)_2^+(Ga_2Cl_7)^-$ (Fig. 2). The use of $GaCl_3$ for the preparation of different radical-cations has been reported in recent literature.[14,15]

The X-ray diffraction analysis showed that crystals conform to a triclinic $P\bar{1}$ space group ($Z = 2$) with a volume of 1569.68(10) Å^3 and no solvent incorporated into the crystal structure. The asymmetric unit contains two crystallographically independent pyrene molecules per one $Ga_2Cl_7^-$ anion. The two pyrene cores show high surface overlap (Fig. 3) with π–π stacking carbon–carbon contacts ranging from 3.326(7) Å to 3.395(7) Å to form the cationic

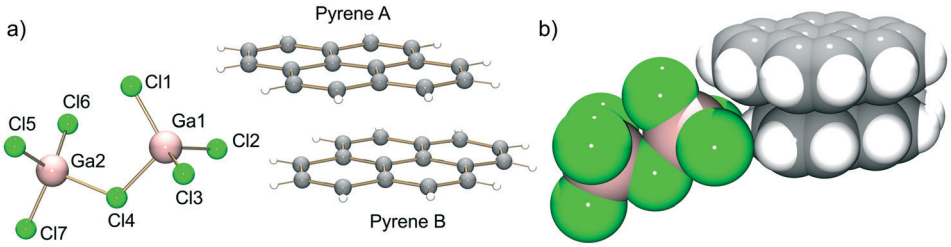

Fig. 2 a) Ball-and-stick and b) space-filling models of $(Py)_2^+(Ga_2Cl_7)^-$.

dimer $(Py)_2^+$. Slightly longer π–π stacking contacts (3.377(7)–3.399(7) Å) are observed between these overlapping dimeric pyrene units, creating π-stacked pyrene columns in the crystallographic *a* direction (Fig. 4). Interestingly, alternating pyrenes are rotated at a 60° angle with respect to the neighboring pyrenes, and this twist is repeated through stacked units (Fig. 3 purple arrows).

In the solid-state structure, each pyrene π-stack is separated by $Ga_2Cl_7^-$ anions, showing alternating columns of cationic and anionic moieties (Fig. 5). Notably different hydrogen bonding contacts are observed between the pyrene cores A and B and $Ga_2Cl_7^-$ anions (Fig. 6). Pyrene B is engaged in multiple H···Cl contacts ranging from 2.810(7) Å to 2.940(7) Å. This is accompanied by a notable C–C bond length elongation at the sites of hydrogen bonding (1.456(1) Å to 1.477(1) Å) from that of the neutral pyrene (1.395(2) Å to 1.401(2) Å). In contrast, pyrene A exhibits fewer contacts (2.841(7) Å) with a less notable effect on the C–C bond lengths (*vide infra*).[16] The observed contacts are consistent with the literature values for H···Cl hydrogen bonding.[17]

The structural deformation of the pyrene core in the crystal structure can be analyzed by C–C bond length and dihedral angle changes (Fig. 6). In pyrene A, the C–C bond lengths at positions r_2 (the bonds highlighted in red) range from 1.397(7) Å to 1.406(7) Å. In contrast, in pyrene B, those bonds in ring β are in the similar range (1.402(6) Å/1.410(6) Å), but a noticeable C–C bond elongation is observed at r_2 in ring α, with values (1.474(6) Å and 1.451(6) Å, respectively) being longer than the common aromatic C–C bonds. Moreover, the dihedral angle between rings α and β in pyrene A is 0.4°, but pyrene B is slightly more curved, with a dihedral angle of 2.6°. This analysis reveals the clear difference between the two pyrene cores in the stacked dimeric unit, which might be indicative of their different charging states (*vide infra*).

Computational methods

Full geometry optimizations have been performed with the UM05-2X/6-311G(d) level of density functional theory (DFT), where U indicates the spin unrestricted version. This combination was shown to provide reliable predictions for pancake bonding among several DFT models[18,19] including a good balance between dispersion interactions and intermolecular electron delocalization which we adopted without further experimentation. No imaginary frequencies were observed for each local minimum. The Gaussian 16 program was used in this work.[20]

The interaction energy, E_{int}, of the dimer is defined as E_{int} = dimer energy at equilibrium − $(E_{monomer}^+ + E_{monomer}^0)$. The

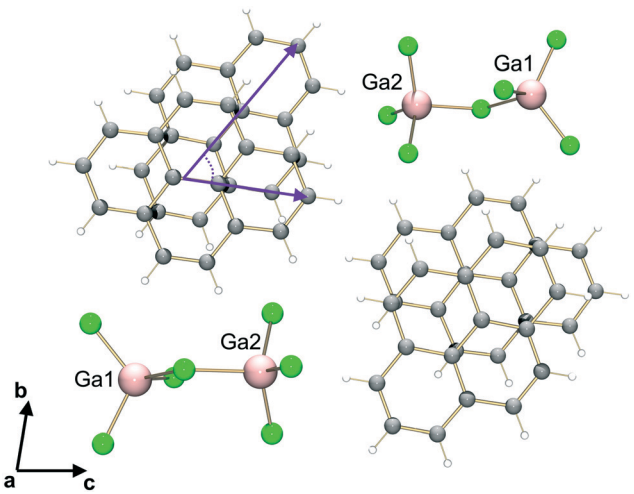

Fig. 3 Overlap of twisting pyrene cores in $(Py)_2^+(Ga_2Cl_7)^-$ down the *a*-axis. The purple arrows and a dashed curved line show the rotation angle.

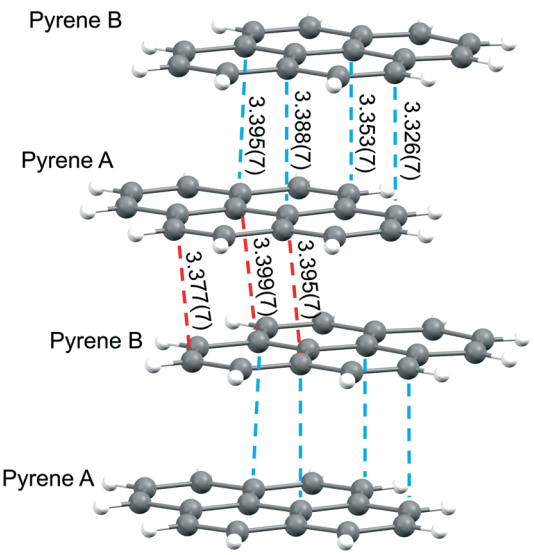

Fig. 4 Interplanar contacts between pyrene molecules.

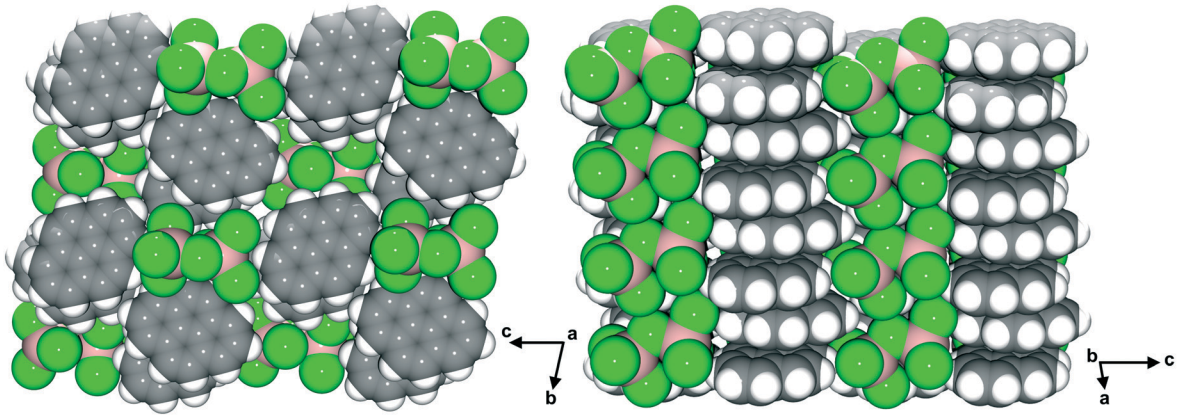

Fig. 5 Solid-state packing of $(Py)_2^+(Ga_2Cl_7)^-$ down the *a*-axis and *b*-axis, space-filling models.

interaction energy in $(Py)_2(Ga_2Cl_7)$ refers to a non-optimized experimental geometry in Table 1.

The assessment of the amount of CT is essential in this work. We have computed the Mulliken atomic charges, using periodic boundary conditions (PBC). Empirically determined charges were obtained from the correlation between computed charges and a bond length alternation (BLA) parameter. Tables S4 and S5† represent comparisons of various PBC methods showing the consistency of the charge distribution among the molecules in the new $(Py)_2(Ga_2Cl_7)$ crystal.

Kistenmacher *et al.*[21] introduced a dimensionless parameter based on the carbon–carbon bond lengths to approximately determine the charge on TCNQ molecules in their charge transfer salts.[22] Here we applied an alternative, using a bond length alternation parameter for pyrene:

$$\mathrm{BLA} = (r_2 + r_5) - 2r_4. \quad (2)$$

This BLA value correlates with the charge on the pyrene molecules and can be used to verify the total charge on various pyrene systems. Fig. S3† displays this correlation purely based on computed optimized geometries on differently charged monomers and dimers of pyrene. This correlation provides a tool to estimate the charge states of various pyrene molecules in charge transfer salts starting from the observed bond lengths.

For the salts of pyrene combined with strong electron acceptors, only the $q > 0$ branch is of interest. The following excellent linear fit has been obtained for this branch consisting of six points:

$$\mathrm{BLA} = 0.0976\ Q - a, \text{ with } a = 0.1279\ (R^2 = 0.9990). \quad (3a)$$

Once established, the inverse relationship is used to estimate charges:

$$Q = 10.236\ \mathrm{BLA} + b, \text{ with } b = 1.3098\ (R^2 = 0.9990). \quad (3b)$$

The neutrality of the unit cells provided a test establishing an approximate error of the pyrene charge of less than $\pm 0.15e$ when eqn (3b) is used ($Q = 0$ is assigned for BLA values more negative than −0.128 Å). In the application of eqn (3b) to the presented new salt and to an iodide salt of pyrene, $(Py)_{10}(I_3^-)_4(I_2)_{10}$ (refcode: BEKQUE[23]) we used a similar correlation with the same slope but an adjusted *b* intercept as discussed in the results section. This correlation has also been cross tested on a series of TCNQ–pyrene complexes for which XRD data are available, as shown in Table S6† where we compare the charges on the pyrenes from eqn (3b) with charges obtained from literature-based data for TCNQ in the same crystal.

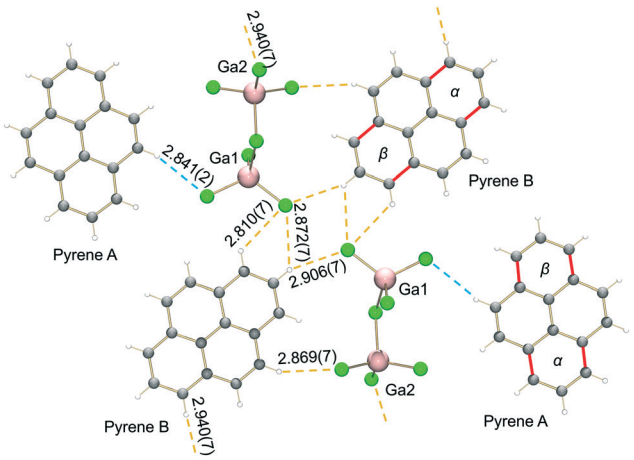

Fig. 6 Hydrogen bonding contacts between pyrene and $Ga_2Cl_7^-$.

Charge localization

The charge distribution between the different pyrene molecules is strikingly uneven as obtained by the PBC computations of this product and shown in Fig. 7, as well as detailed in Tables S4 and S5.† Given the columnar packing of the pyrenes in this crystal, the expectation would be to observe a relatively even distribution of the pyrene charges, $0.5|e|$ on average suggesting a fully delocalized sequence in

Table 1 Six lowest local minima on the PES of $(Py)_2^+$ optimized with UM05-2X/6-311G(d). The relative geometries are represented by *X*, *Y*, *Z*, and θ as illustrated in Fig. 9. Comparative data from cation $(Py)_2^+$ dimers excised from crystal structures are listed in the last six rows

Dimer	*X*, *Y* [in Å], and θ in [°]	Symmetry	Number of over-lapping regions[a]	Average of C···C contacts <3.4 Å [number of contacts]	Computed charge transfer in dimer,[b] [in |e|]	Computed charge transfer in dimer,[c] [in |*e*|]	Dimer interaction energy, [in kcal mol^{-1}]
Minimum 1	0.07, 0.03, 55.0°	D_2	6	3.26 [14]	0.0	0.0	−24.54
Minimum 2	0.06, 1.13, 0.0°	C_{2h}	6	3.26 [7]	0.0	0.0	−22.14
Minimum 3	2.24, 1.07, 0.0°	C_i	4	3.23 [4]	0.0	0.0	−18.24
Minimum 4	2.65, 0.20, 51.8°	C_1	2	3.13 [11]	0.074	0.060	−18.20
Minimum 5	2.17, 1.28, 68.1°	C_1	3	3.31 [11]	0.617	0.805	−17.85
Minimum 6	3.93, 1.15, 52.2°	C_1	2	3.10 [8]	0.095	0.124	−14.35
BEKQUE A[9][d]	0.36, −0.20, 58.5°	C_1	6	3.30 [9]	—	0.185, 0.185	—
BEKQUE A[5][d]	0.15, 1.11, 0.1°	C_1	6	3.32 [5]	—	0.074, 0.075	—
BEKQUE B[7][d]	0.26, −0.28, 58.4°	C_1	6	3.26 [7]	—	0.120, 0.184	—
BEKQUE B[3][d]	0.06, 1.12, 0°	C_1	6	3.36 [3]	—	0.475, 0.412	—
$(Py)_2(Ga_2Cl_7)(Py)_2$[4][f]	2.06, 0.75, 58.1°	C_1	[e]	3.37 [4]	0.870[f]	0.839	−16.800
$(Py)_2(Ga_2Cl_7)(Py)_2$[3][f]	1.87, 0.50, 58.1°	C_1	[e]	3.39 [3]	0.822[f]		−16.760

[a] Each intermolecular bonding orbital region in a pyrene dimer involves two atoms on each of the molecules so as to utilize the bonding regions of the HOMO of the monomer as shown in Scheme 2, *e.g.* regions 4–5, or 5b–6. Orbitals are shown in Fig. S8 and S9.† [b] $|Q_A - Q_B|$ is listed where Q_A and Q_B are the Mulliken charges on the two pyrenes in the dimer and $Q_A + Q_B = 1.0e$. [c] $|Q_A - Q_B|$ is listed where Q_A and Q_B are the charges on the pyrenes calculated from their BLA value from eqn (3b). [d] The four types of neighbor packing geometries in BEKQUE are denoted by the number of short contacts within the two distinct columns of pyrenes in the crystal structure of BEKQUE; which both have the sequence of pyrenes as $(AAAB)_n$ (Table S7†). [e] Orbitals do not show well overlapping regions (Fig. S9†). [f] The value from the 3D full band structure calculation is 0.746 (see Fig. 7 and Table S5†).

the column as $[(Py)^{0.5}(Py)^{0.5+}]_n$ to be contrasted with the PBC computed localized $[(Py)^0(Py)^{1+}]_n$ distribution of charges. This surprising charge localization is an important observation that will be explored below by alternative methods checking the conclusions of this purely theoretical computational result.

Next, we present the analysis of the charge distribution based on the geometries of the molecules first using eqn (2) to obtain the BLA values followed by eqn (3) to obtain the charges on the pyrenes. The parameter *a* in eqn (3a) was adjusted such that the total charge on the two adjacent pyrenes adds up to +1. The charges on the two different pyrene molecules in the $(Py)_2(Ga_2Cl_7)$ structure from this

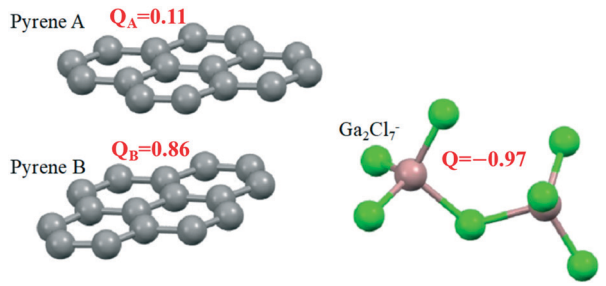

Fig. 7 Total Mulliken molecular charges in red in the unit cell of $(Py)_2(Ga_2Cl_7)$ based on UHF/STO-3G periodic boundary conditions computations. The results for the singlet are shown. For the triplet Q_A = 0 and Q_B = 0.97. For the atomic charges, see Tables S4 and S5.† Note the large difference between Q_A and Q_B.

analysis are shown in Fig. 8. We also added into this diagram two neutral pyrene crystal structures (refcode: GUQPOZ and PYRENE10) and the charge values on each pyrene for a previously known CT iodide salt of pyrene, $(Py)_{10}(I_3^-)_4(I_2)_{10}$ (refcode: BEKQUE). The resulting charge estimate for pyrene A is 0.080, and for pyrene B is 0.920, with Q = −1.0 for the $Ga_2Cl_7^-$ anion; values consistent with the PBC computations summarized in Fig. 7.

A note on the correlations seen in Fig. 8 is in order. The slope reflects the direct correlation between the bonding/antibonding features of the SOMO illustrated in Scheme 2. Two of the pyrenes in $(Py)_{10}(I_3^-)_4(I_2)_{10}$ are assumed to have zero or nearly zero charge: these pyrenes are rather isolated in the unit cell and BLA values (−0.143 and −0.166) are large negative values justifying a zero charge as shown in Fig. 8. Further analysis of these data is presented in the ESI† section providing further evidence for the reliability of using eqn (3) to obtain pyrene charges in its charge transfer salts. The lines for $(Py)_{10}(I_3^-)_4(I_2)_{10}$ and $(Py)_2(Ga_2Cl_7)$ are shifted such that the total charges on all pyrene molecules added together amount to +4 and +1 per unit cell, respectively.

Among the twelve pyrene molecular crystal structures contained in the CSD, PYRENE10 (ref. 16) and GUQPOZ[24] are the most accurate. They represent the BLA values (for GUQPOZ, BLA = −0.118 Å, and for PYRENE10, BLA = −0.129 Å) compared to the theoretical value for the isolated molecule at Q = 0 (BLA = −0.130 Å). Fig. 8 shows how close these two values are to each other and the theoretical value, within less

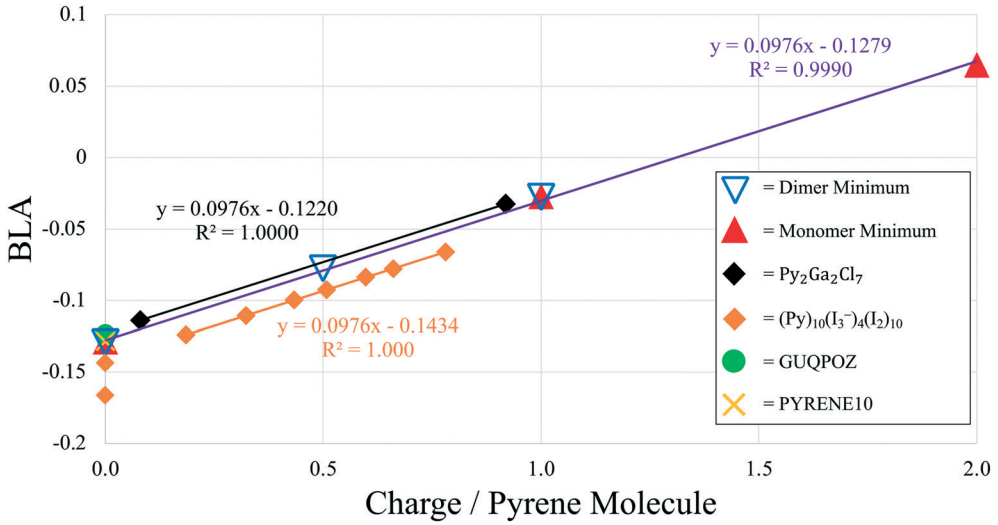

Fig. 8 Bond length alternation, BLA, as a function of charge transfer for computed optimized geometries (triangles) establishes eqn (3a). The inverse eqn (3b) is used to estimate the charges on different pyrenes in the experimental crystals of $(Py)_2(Ga_2Cl_7)$ (present work) and $(Py)_{10}(I_3^-)_4(I_2)_{10}$ (refcode: BEKQUE[8]). BLA values from the most accurate crystal structures of pyrene (CSD refcodes, GUQPOZ[24] and PYRENE10[16]) are indicated at zero charge, $Q = 0$. For explanation, see text.

than 10%. These differences provide an error estimate for this approach translating into an error in the computed charges by eqn (3) of approximately $\pm 0.12|e|$. Further evidence for this approach is provided by its application to the 1 : 1 co-crystal of pyrene–TCNQ, indicating an error of less than $0.15|e|$.

Application of the same approach provided two different BLA values for the two different types of pyrenes from the crystal structure of $(Py)_2(Ga_2Cl_7)$ as follows: −0.114 Å and −0.032 Å. This difference in BLA is very significant and approximately corresponds to the difference in BLA values of neutral and singly charged (+1) pyrene monomers obtained from the DFT optimization with values of −0.129 Å and −0.027 Å, respectively. Again, assuming the same slope of the linear relationship, and total charge of +1 on the dimer, we obtained the two points in Fig. 8 represented by black diamonds.

This estimate is close to the computed charge distribution on the two different pyrenes obtained by the PBC calculations (as listed in Tables S4 and S5†) and is in good agreement with the assumption of a nearly full charge on the $Ga_2Cl_7^-$ anion. While this amount of charge separation of nearly a full electron's charge is surprising, we now find that it is consistent with the molecular structure and with the energy band theory result.

Potential energy surface of $(Py)_2^+$

In what follows we provide an interpretation for the large charge separation between the pyrene molecules in the new charge transfer salt, $(Py)_2(Ga_2Cl_7)$. The nearly complete charge localization is unexpected because these pyrene molecules form a π-stacking geometry which can provide short contacts and good orbital overlap along the 1D stacks. In this case, the short contacts between neighboring pyrenes fall into two categories. We focus on contacts near the van der Waals (vdW) carbon–carbon distance of 3.40 Å as shown in Fig. 4. The shorter contacts are between 3.33 and 3.39 Å and there are four of them, designated as $(Py)_2[4]$. For the other pairs, the distances are between 3.38 and 3.39 Å but there are only three that are shorter than the vdW distance designated as Py[3].

We now turn to the discussion of the potential energy surface (PES) of the cationic pyrene dimer as a model in order to obtain further insights into the molecular packing observed in the new $(Py)_2(Ga_2Cl_7)$ charge transfer salt. Does the observed packing represent a case of ideal or near ideal π-stacking overlap for pancake bonding? The PES of the $(Py)_2^+$ dimer is much more complex than that of the prototypical pancake bonded dimer of phenalenyl, due to the more complex topology of the SOMO as illustrated in Scheme 2. Consequently, a variety of well overlapping parallel π-stacking configurations of the dimer cation exist in which the bonding regions of one pyrene overlap with the other bonding regions in the other pyrene with the appropriate phases. In phenalenyl, only two such configurations exist, and one displays significantly more steric crowding[11] than the other leading to a unique dimer configuration which has been observed in over 50 examples available in the CSD.[25]

Devic *et al.* provided a description of the PES of several cationic dimers of PAHs including $(Py)_2^+$.[8] The geometry is characterized by four parameters illustrated in Fig. 9. They found that the global minimum is at $X = Y = 0$, $\theta = 60°$ corresponding to a well overlapping configuration. Our computation provided the same global minimum, and we identified five additional local minima that are listed in Table 1 and illustrated in Fig. 10, where dimers excised from two experimental structures are also included.

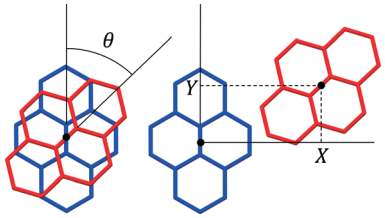

Fig. 9 Definition of parameters used in the pyrene dimer potential energy surface map, rotation θ, and translations X and Y between pyrene centers. The red and blue molecules are displaced in the Z direction maintaining a near parallel orientation. Optimized X, Y, Z, and θ values are listed for local minima in Table 1.

The six local minima on the PES were identified by performing energy minimization starting from a variety of initial structures, partially inspired by the experimental configurations. These minima are characterized by the number of overlapping r_2 and r_5 regions (as defined in Scheme 2) from one pyrene to its neighbor. The numbers of regions with significant orbital overlaps are listed in Table 1; the number of the overlapping regions decreases from six for minima 1 and 2 to two for minimum 6 as the stability of these local minima decreases. The respective important orbital overlaps of $(Py)_2^+$ are shown for these six minima in Fig. S8.†

The comparison of the dimer minima from the computations with those from experiments provides insights. The dimeric PES is characterized by two types of minima: those with parallel ($\theta = 0°$) and rotated (near $\theta = 60°$) dimers. First of course a caveat is in order: the experimental structures contain a stack of pyrene dimers in both $(Py)_{10}(I_3^-)_4(I_2)_{10}$ and $(Py)_2(Ga_2Cl_7)$ crystal structures. For this reason alone, the dimer potential energy surface is a model that can provide only a qualitative guide. It is interesting that the two types of close dimeric contacts in the iodide $(Py)_{10}(I_3^-)_4(I_2)_{10}$ are remarkably close to the two lowest minima as shown in Fig. 10 in terms of the X and Y translations. The respective rotations (θ) are also very close. The two types of dimeric packing in $(Py)_2(Ga_2Cl_7)$ both are near the rotated ($\theta = 60°$) minima. However, the X and Y translations in $(Py)_2(Ga_2Cl_7)$ fall between minimum 5 and minimum 4, albeit this part of the PES is flat, and the two computed minima are within 0.5 kcal mol^{-1} (minimum 3 has similar X and Y translations, but is on the $\theta = 0°$ surface). Given the limitations of any dimer model for a crystal packing analysis, the agreement with experiment is satisfactory.

The nature of electron delocalization between neighboring pyrene molecules is indicative of electron sharing pancake bonding for all six minima listed in Table 1. The strongest corresponds to minimum 1 with the largest (most negative) interaction energy with six nearly perfectly overlapping regions of the SOMOs as illustrated in Fig. 1. Each region corresponds to two π-orbitals each on both pyrenes, which in turn correspond to the six bonding regions in the monomer, as illustrated in Scheme 2. Minimum 2 is nearly as stable (only 2.4 kcal mol^{-1} higher) with similarly six overlapping regions. It is interesting that both minima are utilized by the structure of $(Py)_{10}(I_3^-)_4(I_2)_{10}$ with a relatively small deviation from the experimental structures for the minima as illustrated in Fig. 10. These two are clear cases of a one-electron pancake bonding with the formal pancake bond order of 1/2. The discussion of these and similar structures led Devic *et al.* to their maximin principle of highly overlapping π-stacking interactions.[8]

Further four minima were found during the optimization of the geometry of $(Py)_2^+$ as listed in Table 1 in the order of

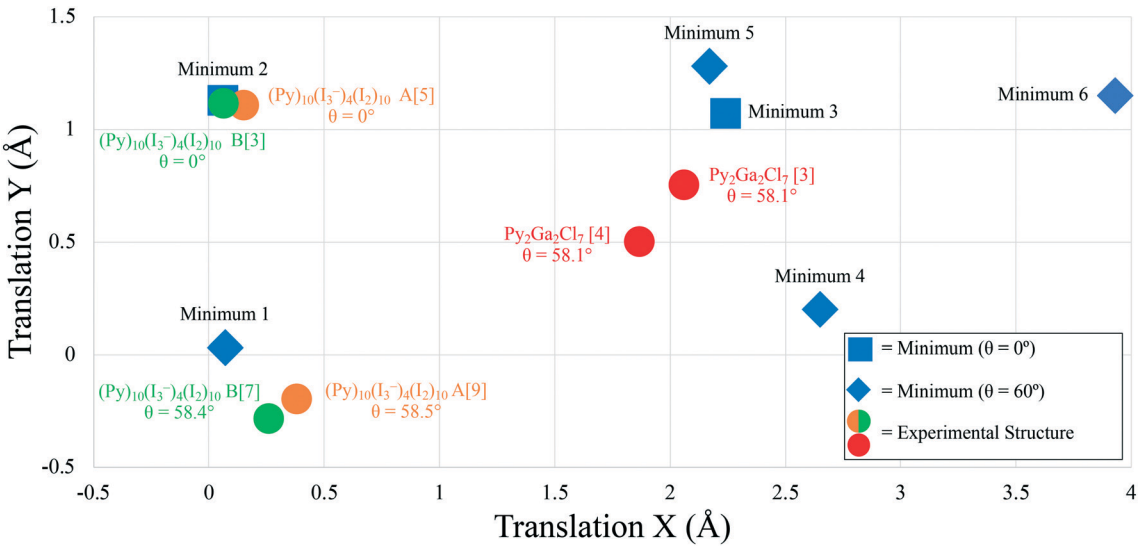

Fig. 10 Potential energy surface map for the mono-cationic pyrene dimer, $(Py)_2^+$. Computed data of the six local minima listed in Table 1 are shown in blue marks. Experimental dimeric structures excised from the presented $(Py)_2(Ga_2Cl_7)$ crystal and from $(Py)_{10}(I_3^-)_4(I_2)_{10}$ (ref. 23) are indicated as red and orange or green circles, respectively. Note that each green/orange circle pair refers to $(Py)_{10}(I_3^-)_4(I_2)_{10}$ corresponding to two virtually identical dimers.

decreasing interaction energy and are further illustrated in Fig. 10 together with respective data on the two types of dimers found in $(Py)_2(Ga_2Cl_7)$. Two of the minima (minima 2 and 3) correspond to near $\theta = 0°$, the other four to near $\theta = 60°$. This is interesting and provides validation that the dimers excised from the iodide salt $(Py)_{10}(I_3^-)_4(I_2)_{10}$ correspond to the two lowest minima of dimers $(Py)_2^+$ PES (minima 1 and 2). In stark contrast the presented new $(Py)_2(Ga_2Cl_7)$ dimer structures are between minima 4 and 5.

The dimer computations show significant charge separation between the two pyrenes in some of the dimer configurations even without the inclusion of the counterions. This localization effect is most pronounced in minimum 5, and to a lesser degree for minima 6 and 4. These three optimized geometries with charge separation correspond to a rotated intermolecular geometry near $\theta = 60°$. The charge separation obtained in both the 3D band structure calculation and the charge obtained from BLA has been discussed above. The charge separation in the isolated dimers supports these findings further.

Notably, the two different pyrene dimers in the crystal structure of $(Py)_2(Ga_2Cl_7)$, namely $(Py)_2[3]$ and $(Py)_2[4]$, are close to the ideal relative rotation of $\theta = 60°$. However, both the *X* and *Y* translations place these structures significantly away from the nearby energy minima of minimum 4 and minimum 5 (minimum 3 with $\theta = 0°$ is far in configuration space). It is noteworthy that for minimum 5 the overlap is less than ideal, as indicated by the significant charge separation for that minimum as listed in Table 1. The orbitals for the $(Py)_2^+$ for minimum 5 show very little pyrene-to-pyrene overlap.

Pancake bonding and uneven charge distribution

The charge localization observed here is completely different from those seen in some 1/3 and 2/3 filled charge transfer salt crystals (filling refers to the charge per π-stacking molecule divided by two referring to the filling of the π-electron derived energy band). An early example for a 1/3 filled case is $[TCNB]_3^{2-}$ (TCNB is tetracyanobenzene) in its CT salt.[26] Here, as in other similar cases, the two electrons transferred to a π-stacking trimer of the acceptors are delocalized over the well overlapping pancake bonding π-orbitals. In analogy to the lowest π-orbital of allyl, the distribution is uneven, the largest contribution being on the central atom in allyl and on the central TCNB in the CT salt. Other cases of a similar charge distribution have been discussed along these lines as well, for example a salt of tetrachloroquinone, $[Cl_4Q]_3^{2-}$ anion, is also describable similarly with an uneven charge distribution obtained both experimentally and by quantum chemical computations.[10] On the other hand, a more pronounced charge localization was observed by Dunbar *et al.*[27] for a CT salt of $[TCNQ]_3^{2-}$ which can be described approximately as $[(TCNQ^0)\ (TCNQ^-)_2]$ with charges based on Kistenmacher's charge-bond length correlation.[21] Herbstein and Kapon have reviewed the literature[4] on columnar salts of TCNQ highlighting that X-ray crystallography can favorably identify charge localization of the kind of $[(TCNQ)^0\ (TCNQ)^{1-}]_n$.

Based on the strong evidence discussed above, the charge distribution among the pyrenes in the presented $(Py)_2(Ga_2Cl_7)$ salt is significantly uneven, suggesting an approximate $(Py)(Py^+)$ sequence in the columnar stacks rather than the even or nearly even distribution of approximately $(Py^{1/2+})(Py^{1/2+})$.

For strong pancake bonding to occur, a favorable intermolecular π–π overlap is necessary. This interaction is available for minima 1, 2, and 3 resulting in relatively strong intermolecular interactions with even charge distribution between the two pyrenes, as listed in Table 1. The favorable bonding intermolecular interactions are seen for at least one dimer orbital based on the molecular π-orbitals in each of these three cases providing six or four regions of bonding intermolecular interactions as shown in Fig. S8.† Moving down Table 1 to minima 4, 5, and 6, the interaction energy is reduced, the number of overlapping regions is reduced to three or two and most importantly a spontaneous substantial charge separation occurs, most pronouncedly for minimum 5, for which the computed amount of charge separation is not complete, but corresponds to $Q_A = 0.81$, and $Q_B = 0.19$ by Mulliken population analysis. The charge difference computed from the BLA by eqn (3) is similar: $Q_A = 0.90$, $Q_B = 0.10$, a nearly complete charge transfer value by both methods.

The large BLA difference is clear evidence of a large bond relaxation responding to the localized charge in a manner similar to a static polaron. In this case (minimum 5) the relevant orbitals show minimum overlap between the two pyrenes (see Fig. S8†), consistent with a weaker intermolecular interaction. In this case pancake bonding is not present, the total intermolecular interaction should be traced back to vdW interactions, *i.e.*, dispersion and electrostatics. Note that the electrostatic interaction can be attractive and significant in π-stacking positively charged dimers of PAHs,[11] accounting for the relatively large interaction energies seen in Table 1 for the $(Py)_2^+$ species.

The key points of this discussion on the dimer models can be transferred with modifications to the pyrene–pyrene interactions in the new $(Py)_2(Ga_2Cl_7)$ salt. While the pyrenes in the salt do not form singly charged well-isolated dimers, the geometries of each adjacent pyrene pair have a less than ideal packing for the kind of overlap necessary for pancake bonding, as exemplified by minima 1, 2, and 3 on the PES shown in Fig. 10. Clearly for reasons of crystal packing, the actual structure of the salt shows neighbor configurations between minimum 4 and minimum 5 on the $\theta = 60°$ PES. Consequently, the spontaneous charge localization proceeds along the lines of that of minimum 5. Localization is further enabled by the additional reduction of the pyrene–pyrene overlap given the mismatch of the actual overlap (the *X* and *Y* slip values are different) in the salt compared to minimum 5. Virtually zero intermolecular overlap is seen in all relevant orbitals shown in Fig. S9† for the pyrene dimers excised from the crystal structure of $(Py)_2(Ga_2Cl_7)$ for both the $(Py)_2[3]$ and $(Py)_2[4]$ configurations.

The uneven distribution of the position of chlorides in the crystal structure may suggest that the negative charges that they represent are at the origin or enhance the charge localization of the positive charges on every other pyrene. In an additional computational modeling the anions were represented with point charges at four Cl^- sites closest to the pyrenes with fixed geometry excised from the crystal structure. Three $(Py)_2^+$ configurations were considered: $(Py)_2$[3], $(Py)_2$[4] where significant charge transfer occurs and at the geometry of minimum 1 where no charge transfer occurs. Charge transfer values between the two pyrenes in the dimer were computed as a function of the point charge values, q_{Cl}, at the locations of the chloride atoms and are summarized in Fig. S7.† The charges even at large values above $q_{Cl} = -0.5|e|$ indicate no significant change in the value of the charge transfer, $\Delta Q = |Q_A - Q_B|$. This computational modeling shows that the effect of external charges provides at most a small modification of the charge localization and cannot be considered as the main source of charge localization in $(Py)_2(Ga_2Cl_7)$. We conclude that the charge localization in the pyrene stacks is due to the relative positions of the pyrenes observed in the crystal structure that does not permit sufficiently large overlap which would allow charge delocalization along the π-stacks. The energy cost of such a low degree of intermolecular overlap is likely compensated by crystal packing.

Conclusions

Particularly fascinating are crystal structures, where organic conjugated molecules have more than one significantly different molecular environment and this occurs in the new CT crystal structure of pyrene, $(Py)_2^+(Ga_2Cl_7)^-$, as well. The unit cell contains two chemical repeat units, each of which contains an odd number of electrons. Materials with this property can be candidates for organic metallic-like systems or systems with interesting magnetic properties and deserve attention.

The observed significant differences in the bond length alternation values between the two crystallographically inequivalent pyrene molecules have been linked to molecular charges indicating a large degree of charge localization on one of the two pyrenes in the new $(Py)_2^+(Ga_2Cl_7)^-$ salt. This conclusion is strongly supported by evidence from crystal structure analysis as well as calculations on dimer models of $(Py)_2^+$ excised from the crystal structure of both the new salt and the $(Py)_{10}(I_3^-)_4(I_2)_{10}$ iodide salt. Further supported by energy minimization on the molecular cations $(Py)_2^+$ we find that a number of pancake bonding structures should exist on the potential energy surface. However, in the presented crystal structure, due to crystal packing effects (which cannot be fully modeled by computational methods), the actual dimer packing is not sufficiently close to any of these minima to ensure full pancake bonding. We conclude that very limited electron delocalization can be identified in the newly reported crystal structure in agreement with the concluded charge localization.

Author contributions

Z. Z. and M. E. M. crystallized the product, completed its structural description, and contributed to the manuscript preparation; Z. W. performed the X-ray data collection and refinement: M. A. P. supervised the experimental part of this work and contributed to the discussion of the results and manuscript preparation with the support and contribution of all authors; C. F. participated in the analysis of the computational data and performed most of the computations; M. K. supervised the computational part of this work and contributed to the analysis and discussion of the results and manuscript preparation.

Conflicts of interest

There are no conflicts to declare.

Acknowledgements

Support by the U. S. National Science Foundation for this research, CHE-2107820 (M. K.) and CHE-2003411 (M. A. P.), is gratefully acknowledged.

References

1 J. B. Torrance, The Difference Between Metallic and Insulating Salts of Tetracyano-quinodimethone (TCNQ): How to Design an Organic Metal, *Acc. Chem. Res.*, 1979, **12**, 79–86.
2 R. M. Metzger and A. N. Bloch, Crystal Coulomb Energies. VII. The Electrostatic Binding Energy Defect in Tetrathiofulvalinium 7, 7, 8, 8,-tetracyanoquinodimethanide, *J. Chem. Phys.*, 1975, **63**, 5098–5107.
3 Z. G. Soos, Theory of π-Molecular Charge-Transfer Crystals, *Annu. Rev. Phys. Chem.*, 1974, **25**, 121–153.
4 F. H. Herbstein and M. Kapon, Classification of closed shell TCNQ salts into structural families and comparison of diffraction and spectroscopic methods of assigning charge states to TCNQ moieties, *Crystallogr. Rev.*, 2008, **14**, 3–74.
5 K. E. Preuss, Pancake Bonds: π-Stacked Dimers of Organic and Light-Atom Radicals, *Polyhedron*, 2014, **79**, 1–15.
6 M. Kertesz, Pancake Bonding: An Unusual Pi-Stacking Interaction, *Chem. – Eur. J.*, 2019, **25**, 400–416.
7 D. E. Schafer, F. Wudl, G. A. Thomas, J. P. Ferraris and D. O. Cowan, Apparent Giant Conductivity Peaks in an Anisotropic Medium: TTF-TCNQ, *Solid State Commun.*, 1974, **14**, 347–351.
8 T. Devic, M. Yuan, J. Adams, D. C. Fredrickson, S. Lee and D. Venkataraman, The Maximin Principle of π-Radical Packings, *J. Am. Chem. Soc.*, 2005, **127**, 14616–14627.
9 Z.-H. Cui, H. Lischka, H. Z. Beneberu and M. Kertesz, Double Pancake Bonds: Pushing the Limits of Strong π-π Stacking Interactions, *J. Am. Chem. Soc.*, 2014, **136**, 12958–12965.

10 K. Molčanov, Z. Mou, M. Kertesz, B. Kojić-Prodić, D. Stalke, S. Demeshko, A. Šantić and V. Stilinović, Pancake Bonding in π-Stacked Trimers in a Salt of Tetrachloroquinone Anion, *Chem. – Eur. J.*, 2018, **24**, 8292–8297.

11 Z.-H. Cui, M. H. Wang, H. Lischka and M. Kertesz, Unexpected Charge Effects Strengthen π-Stacking Pancake Bonding, *JACS Au*, 2021, **1**, 1647–1655.

12 D. Small, V. Zaitsev, Y. S. Jung, S. V. Rosokha, M. Head-Gordon and J. K. Kochi, Intermolecular, Pi-to-Pi Bonding Between Stacked Aromatic Dyads. Experimental and Theoretical Binding Energies and Near-IR Optical Transitions for Phenalenyl Radical/Radical Versus Radical/Cation Dimerizations, *J. Am. Chem. Soc.*, 2004, **126**, 13850–13858.

13 K. Goto, T. Kubo, K. Yamamoto, K. Nakasuji, K. Sato, D. Shiomi, T. Takui, M. Kubota, T. Kobayashi, K. Yakusi and J. Ouyang, A Stable Neutral Hydrocarbon Radicals: Synthesis, Crystal Structure, and Physical Properties of 2,5,8-Tri-*tert*-butyl-phenalenyl, *J. Am. Chem. Soc.*, 1999, **121**, 1619–1620.

14 M. Y. Abraham, Y. Wang, Y. Xie, R. J. Gilliard Jr, P. Wei, B. J. Vaccaro, M. K. Johnson, H. F. Schaefer III, P. V. R. Schleyer and G. H. Robinson, Oxidation of Carbene-Stabilized Diarsenic: Diarsene Dications and Diarsenic Radical Cations, *J. Am. Chem. Soc.*, 2013, **135**, 2486–2488.

15 R. Kinjo, B. Donnadieu, M. A. Celik, G. Frenking and G. Bertrand, Synthesis and Characterization of a Neutral Tricoordinate Organoboron Isoelectronic with Amines, *Science*, 2011, **333**, 610–613.

16 A. Matsumoto, M. Suzuki, H. Hayashi, D. Kuzuhara, J. Yuasa, T. Kawai, N. Aratani and H. Yamada, Aromaticity Relocation in Perylene Derivatives upon Two-Electron Oxidation to Form Anthracene and Phenanthrene, *Chem. – Eur. J.*, 2016, **22**, 14462–14466.

17 C. B. Aakeroy, T. A. Evans, K. R. Seddon and I. Palinko, The C-H···Cl Hydrogen Bond: Does it Exist?, *New J. Chem.*, 1999, **23**, 145–152.

18 S. N. Steinmann, C. Piemontesi, A. Delachat and C. Corminboeuf, Why are the Interaction Energies of Charge-Transfer Complexes Challenging for DFT?, *J. Chem. Theory Comput.*, 2012, **8**, 1629–1640.

19 Z. Mou, Y.-H. Tian and M. Kertesz, Validation of Density Functionals for Pancake Bonded π-Dimers; Disperison is not Enough, *Phys. Chem. Chem. Phys.*, 2017, **19**, 24761–24768.

20 M. J. Frisch, G. W. Trucks, H. B. Schlegel, G. E. Scuseria, M. A. Robb, J. R. Cheeseman, G. Scalmani, V. Barone, G. A. Petersson, H. Nakatsuji, X. Li, M. Caricato, A. V. Marenich, J. Bloino, B. G. Janesko, R. Gomperts, B. Mennucci, H. P. Hratchian, J. V. Ortiz, A. F. Izmaylov, J. L. Sonnenberg, D. Williams-Young, F. Ding, F. Lipparini, F. Egidi, J. Goings, B. Peng, A. Petrone, T. Henderson, D. Ranasinghe, V. G. Zakrzewski, J. Gao, N. Rega, G. Zheng, W. Liang, M. Hada, M. Ehara, K. Toyota, R. Fukuda, J. Hasegawa, M. Ishida, T. Nakajima, Y. Honda, O. Kitao, H. Nakai, T. Vreven, K. Throssell, J. A. Montgomery Jr., J. E. Peralta, F. Ogliaro, M. J. Bearpark, J. J. Heyd, E. N. Brothers, K. N. Kudin, V. N. Staroverov, T. A. Keith, R. Kobayashi, J. Normand, K. Raghavachari, A. P. Rendell, J. C. Burant, S. S. Iyengar, J. Tomasi, M. Cossi, J. M. Millam, M. Klene, C. Adamo, R. Cammi, J. W. Ochterski, R. L. Martin, K. Morokuma, O. Farkas, J. B. Foresman and D. J. Fox, *Gaussian 16, Rev.A.03*, Gaussian, Inc., Wallingford CT, 2016.

21 T. J. Kistenmacher, T. E. Phillips and D. O. Cowan, The Crystal Structure of the 1:1 Radical Cation–Radical Anion Salt of 2,2′-Bis-l,3-Dithiole (TTF) and 7,7,8,8-Tetracyanoquinodimethane (TCNQ), *Acta Crystallogr., Sect. B: Struct. Crystallogr. Cryst. Chem.*, 1974, **30**, 763–768.

22 R. Sanada, D. Yoo, R. Sato, K. Iijima, T. Kawamoto and T. Mori, Ambipolar Properties of Charge-Transfer Complexes Containing Perylene and Dicyanoquinonediimines, *J. Phys. Chem. C*, 2019, **123**, 12088–12095.

23 S. Lee, B. Chen, D. C. Fredrickson, F. J. DiSalvo, E. Lobkovsky and J. A. Adams, Crystal Structures of $(Pyrene)_{10}(I_3^-)_4(I_2)_{10}$ and $[1,3,6,8\text{-Tetrakis(Methylthio)Pyrene}]_3(I_3^-)_3(I_2)_7$: Structural Trends in Fused Aromatic Polyiodides, *Chem. Mater.*, 2003, **15**, 1420–1433.

24 X. Pang, H. Wang, W. Wang and W. J. Jin, Phosphorescent π-Hole···π Bonding Cocrystals of Pyrene with Hal-perfluorobenzenes (F, Cl, Br, I), *Cryst. Growth Des.*, 2015, **15**, 4938–4945.

25 Z.-H. Cui, A. Gupta, H. Lischka and M. Kertesz, Concave or Convex π-Dimers: The Role of the Pancake Bond in Substututed Phenalenyl Radical Dimers, *Phys. Chem. Chem. Phys.*, 2015, **17**, 23963–23969.

26 J. D. Bagnato, W. W. Shum, M. Strohmeier, D. M. Grant, A. M. Arif and J. S. Miller, The Structure of Fractionally Charged Tetracyanobenzene^{n-} Present in $[TCNB]_3^{2-}$, *Angew. Chem.*, 2006, **118**, 5448–5452.

27 X. Zhang, Z. X. Wang, H. Xie, M. X. Li, T. J. Woods and K. R. Dunbar, A Cobalt (II) Spin-Crossover Compound with Partially Charged TCNQ Radicals and an Anomalous Conducting Behavior, *Chem. Sci.*, 2016, **7**, 1569–1574.

